

Current Biology

Complex Pattern Selectivity in Macaque Primary Visual Cortex Revealed by Large-Scale Two-Photon Imaging

Highlights

- V1 neuronal responses were studied by using two-photon imaging in awake monkeys
- Large population of V1 neurons responded to thousands of visual stimuli
- V1 superficial layer neurons exhibited high selectivity to complex patterns

Authors

Shiming Tang, Tai Sing Lee, Ming Li, ..., Fang Liu, Benjamin Teo, Hongfei Jiang

Correspondence

tangshm@pku.edu.cn (S.T.),
tai@cnbc.cmu.edu (T.S.L.)

In Brief

Tang et al. performed large-scale two-photon imaging in awake monkeys and found a large percentage of V1 neurons exhibited complex pattern selectivities.

Complex Pattern Selectivity in Macaque Primary Visual Cortex Revealed by Large-Scale Two-Photon Imaging

Shiming Tang,^{1,2,3,5,*} Tai Sing Lee,^{4,*} Ming Li,^{1,2,3} Yimeng Zhang,⁴ Yue Xu,⁴ Fang Liu,^{1,2,3} Benjamin Teo,⁴ and Hongfei Jiang^{1,2,3}

¹Peking University School of Life Sciences and Peking-Tsinghua Center for Life Sciences, Beijing 100871, China

²IDG/McGovern Institute for Brain Research at Peking University, Beijing 100871, China

³Key Laboratory of Machine Perception (Ministry of Education), Peking University, Beijing 100871, China

⁴Center for the Neural Basis of Cognition and Computer Science Department, Carnegie Mellon University, Pittsburgh, PA 15213, USA

⁵Lead Contact

*Correspondence: tangshm@pku.edu.cn (S.T.), tai@cnbc.cmu.edu (T.S.L.)

<https://doi.org/10.1016/j.cub.2017.11.039>

SUMMARY

Visual objects contain rich local high-order patterns such as curvature, corners, and junctions. In the standard hierarchical model of visual object recognition, V1 neurons were commonly assumed to code local orientation components of those high-order patterns. Here, by using two-photon imaging in awake macaques and systematically characterizing V1 neuronal responses to an extensive set of stimuli, we found a large percentage of neurons in the V1 superficial layer responded more strongly to complex patterns, such as corners, junctions, and curvature, than to their oriented line or edge components. Our results suggest that those individual V1 neurons could play the role in detecting local high-order visual patterns in the early stage of object recognition hierarchy.

INTRODUCTION

Neurophysiological studies in the past 60 years have provided a wealth of understanding of the functions and codes of the mammalian primary visual cortex. V1 neurons are understood to exhibit tunings to many basic visual attributes, such as orientation, color, and motion directions [1–4]. In addition, they are subject to a variety of contextual modulations [5, 6].

In the domain of contour or form encoding, it is often believed that V1 neurons primarily serve as simple oriented feature detectors and that subsequent visual areas take conjunctions of these elements to construct higher-order (HO) feature detectors, gradually building up feature selectivity to more complex and global patterns along the ventral visual pathway [7–10]. This hierarchical architecture for object recognition was the inspiration for deep convolutional neural networks in machine learning [11, 12].

However, evidence from numerous earlier studies suggests that V1 neuronal codes might be more complex and nuanced. In fact, Hubel and Wiesel found many hypercomplex cells in the superficial layer of V1 were difficult to characterize [1, 13],

and these were later characterized by their end-stopping property. Some studies suggested that end-stopping could be used to compute curvature in V1 [14, 15]. Other studies suggested that V1 neurons may also be coding complex features [16, 17], and their responses were often difficult to model or interpret particularly when stimulated with more complicated or natural stimuli [18, 19]. Moreover, possible biases in neuron sampling, as well as a limited number of tested stimuli, prevented us from a full understanding of the V1 neuronal functions [20, 21].

Recent developments in large-scale two-photon calcium-imaging techniques [22, 23] in awake monkeys make it possible to characterize the V1 neuron tunings more thoroughly, reducing the sampling bias and cell-sorting errors common in conventional single- and multi-electrode recording studies [20, 23]. This allows us to more thoroughly check the selectivity and specificity of the neurons' tunings by testing an extensive set of visual shape features, including orientations, corners, junctions, curvatures, crosses, concentric gratings, and composite features.

Our results revealed that a large percentage of V1 neurons in the superficial layer exhibit strong selectivities to specific complex features. While most of these neurons tended to respond mildly to oriented gratings and bars, and thus exhibited some degree of orientation tuning, they responded much more strongly to their favorite complex patterns. The high degree of specificity in these neurons' pattern selectivity suggests that they might serve as specific pattern detectors for detecting and signaling the presence of corners, curves, junctions, as well as other ecologically meaningful patterns, which could have profound implications for the construction of visual object recognition hierarchy.

RESULTS

Two-Photon Calcium Imaging of V1 Superficial Layer Neurons in Awake Monkeys

We performed large-scale, two-photon imaging of neuronal populations in the V1 superficial layer of awake monkeys (*Macaca mulatta*) with calcium indicator GCaMP5 [23, 24] derived by adeno-associated virus (AAV) (Figures 1A and 1B). The V1 neurons' calcium signals in response to visual stimuli were imaged with a two-photon microscopic technique while

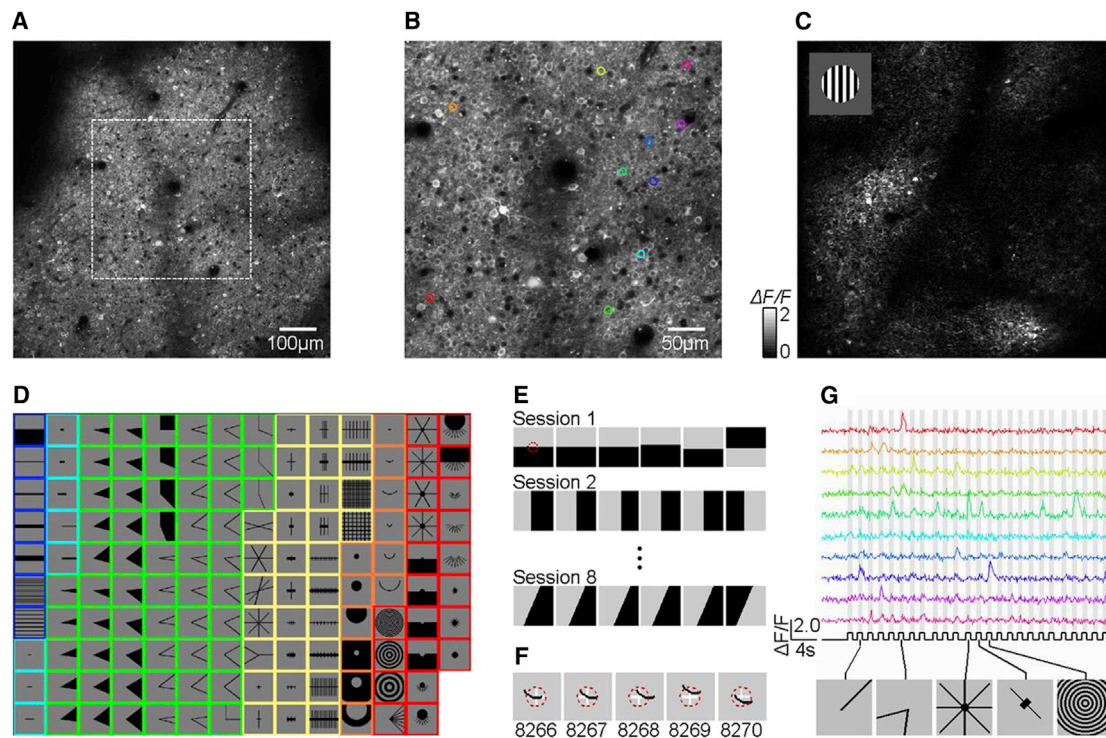


Figure 1. Large-Scale Two-Photon Calcium Imaging and Visual Pattern Scanning in Awake Monkeys

(A and B) Two-photon images from the macaque primary visual cortex infected by AAV1-GCaMP5G, zoomed 1× (A) and 2× (B).

(C) An example of differential images from monkey B showing the neuronal population response to a drifting grating.

(D) The basic prototype patterns used for the generation of the 9,500 stimulus set. The standard orientation (OT) stimuli included edges, long and short bars (0.4°, 0.6°, and 1° in length and 0.1° and 0.2° in width), and gratings. The HO stimuli included corners, curvatures, crosses, and composition patterns such as plaids, rings rays, and whiskers, which were the combinations or variations of the simpler stimuli.

(E) The stimulus sets were generated by rotating the basic patterns in 22.5° steps and are presented at five position placements. Each rotation was tested in one single session.

(F) Each stimulus was presented at the cluster center of all the neurons' receptive field, as well as four positions with 0.2° displacements from the center in the four cardinal directions. The red dashed circles indicate the 0.8° diameter of aggregated RFs of the neuronal population. The white crosses indicate the averaged center of RFs for all imaged neurons.

(G) Raw calcium signal traces of the ten example cells marked in color code in (B) in response to the visual stimuli.

See also [Figures S1](#) and [S2](#) and [Movie S1](#).

the monkeys performed a fixation task. In each trial, the monkeys maintained fixation for at least 2 s to get a juice reward. During each fixation, a blank screen was presented for 1 s, followed by a visual stimulus for another second. To quantify the neural responses, a differential image of the calcium signals between the stimulus period and the blank period was computed for each trial (Figure 1C). The regions of interest (ROIs) of activated cells were identified from the differential images. The response of a cell was computed as the standard $\Delta F/F_0$, based on the averaged activity within an ROI during stimulus presentation in each trial (see [STAR Methods](#)).

An 850 × 850 μm imaging field was located at a retinal eccentricity of 3° to 4° (in visual angles) for each monkey. The cortical depth being imaged was from 160 to 180 μm, which was within the superficial layers of V1. The imaged area typically spans one to two hypercolumns, with recognizable pinwheel orientation maps [23]. The receptive fields of the neurons were first localized with small oriented gratings (Figure 1C). They were then mapped precisely with short black/white bars of six orientations and small black/white squares. The sizes of the neurons' receptive fields

(RFs) that can be mapped out by the short bars varied from 0.5° to 0.8° in diameter. The receptive fields of the neurons form a relatively tight cluster with aggregated spatial coverage spanning about 1.0° because they were mostly from one or two hypercolumns.

Experimental and Stimulus Designs

We tested the neurons' responses to a diverse set of simple and complex stimuli, generated from 138 basic prototypes (Figure 1D). These prototypes were grouped into five major categories (color marked in Figure 1D): orientation (OT) stimuli (edges, bars, and gratings), corner (CN) stimuli, curvature (CV) stimuli, cross (CX) stimuli, and composition (CO) stimuli (composition patterns created by combining multiple elements drawn from the first four categories). The CO stimuli were found to be effective in driving the neurons in our pilot experiments. Each of the stimuli was shown in a 3° × 3° aperture. Notably, some patterns had relatively small sizes (comparable to the size of receptive fields of the imaged neurons), including short-oriented bars (0.4°, 0.6° and 1° in length) and smallest CV stimuli in

column 12 (see [Figure 1D](#)). A comprehensive presentation of the CV and CN stimuli tested is presented in [Figure S1](#).

The stimulus set was designed to test the hypothesis that neurons in V1 are not only orientation tuned but also selective to specific HO features. As a HO feature could contain multiple lower-order features (e.g., locally oriented bars) as its components, testing this hypothesis involves testing a neuron's selective responses to a HO pattern as well as its oriented component parts.

In the full set of stimuli, each of these 138 prototypes was rotated in increments of 22.5° , resulting in eight rotations for symmetric and 16 rotations for asymmetric patterns (see [Figure 1E](#)). Each stimulus was presented in five spatial positions—one at the center of the receptive field clusters and four at a 0.2° shift in each of the cardinal directions (see [Figure 1F](#)). Since the aggregated receptive field of the imaged neurons at 3° eccentricity covered about 0.8° in diameter, testing stimuli at those five spatial positions over the aggregated receptive field maximized the probability of presenting stimuli at the center of the receptive fields of the individual imaged neurons.

The entire stimulus set consisted of 1,600 standard orientation patterns, including edges, short and long bars, and gratings, and 7,900 more complex HO patterns (curvatures, corners, crosses, and composition patterns). The stimulus set was similar to that in earlier studies for characterizing complex pattern selectivity of V2 and V4 neurons with single-unit recording [16], except that our stimulus set covered the feature space more extensively and contained more control stimuli for assessing local and global orientation tuning and end-stopping tuning properties.

The stimulus set was divided into eight subsets. Each was associated with one of the eight major rotations of the 138 prototypes in 22.5° increments and was tested in a single, one-day session in about 6,000 trials ([Figures 1E](#) and [1F](#)). Stimulus presentations were randomly interleaved. Each stimulus was repeated five to six times. The responses of each individual neuron indicated by the calcium signal during stimulus presentation were extracted and analyzed ([Figure 1G](#)).

To reduce the bias in cell sampling, we identified all activated cells automatically based on their visual responses (ROIs with activities above 3 SD of the differential images) to all visual stimuli tested. We identified 1,142 activated cells in monkey A and 979 cells in monkey B. Weakly responding cells with peak $\Delta F/F0 < 0.5$ were excluded from further analysis because of the relatively large noises and uncertainty concerning their actual stimulus preference. The responses of the remaining 767 and 816 cells from monkeys A and B were analyzed, respectively.

Our previous study showed that, with high-quality image registration, single cells could be tracked reliably (>90% cells across days to weeks) and their neuronal responses were stable across days [23] (see also [Figure S2](#) and [Movie S1](#)). To confirm the quality of image registration and the stability of neuronal responses in this study, we repeated a set of stimuli in every recording session. We found that the neuron responses were stable across days ([Figure S2](#)). These results confirm both the high quality of image registration and the stability in recordings across days. Signals extracted from all image series were combined into an integrated neuronal response matrix to all the 9,500 tested visual stimuli for further analysis. We were able to test the complete set in monkey A. However, we were only able to test a coarser set

(four major orientations at 45° rotation increments, totaling 4,605 stimuli) in monkey B across 4 days before we lost precise image registration of some of the tracked neurons. Even so, the dense-oriented bars (7.5° or 48 orientations) were tested in both monkeys. The results from monkey B did not differ significantly from our key results from monkey A on pattern selectivity.

Neuronal Selectivity to Specific Complex Patterns

We observed that a large percentage of imaged V1 neurons responded significantly stronger to high-order, complex patterns (HO stimuli) than to standard oriented bars and gratings (OT stimuli). In one example from monkey A, distinct neuronal populations were activated by a particular curvature as well as by bars of two different orientations ([Figures 2A–2C](#); see also [Movie S2](#)). Among these, cell 554 responded strongly to the CV stimuli ([Figure 2D](#)) but only weakly to any of the oriented bars. Furthermore, among the 9,500 stimuli tested, all of the preferred stimuli of this cell (with $\Delta F/F0$ above half of the maximum response observed for this neuron) belonged to the curvature category ([Figure 2D](#)). This neuron did not respond well to bars of different orientations in different lengths ([Figure 2E](#)).

To confirm that the high degree of selectivity to specific curvature patterns was not due to spurious activities of neurons or unknown sources of variability in the system, we performed receiver operating characteristic (ROC) analysis [25] across trials for each neuron ([Figure 2F](#)) and compared with that from trials obtained by shuffling stimulus labels in each trial. The much higher area under the ROC curve (AUC) from observed data (close to 1.0) than that from shuffled data (around 0.67) indicated that this neuron's responses to its preferred stimuli were highly reliable across trials and could not have arisen from chance ($p < 0.001$; see [STAR Methods](#) and [Figure S3](#)).

As in the case of cell 554, when a cell's preferred stimuli (i.e., with responses above half of its maximum) all belonged to the curvature category or composition patterns that contained curvatures, it was classified as a curvature-selective cell. In total, we found 57 curvature-selective cells in monkey A and 53 in monkey B. All but four cells passed the ROC significance test ($p < 0.001$), while those four cells passed the test with $p < 0.05$, indicating a high degree of reliability in their selective responses to CV stimuli across trials.

Note that these curvature-selective cells are qualitatively different from the cells with curvature tunings reported in previous studies [14, 15]. Cells with curvature tuning, reported earlier, could respond equally well to both short-oriented bars and preferred curvatures. The curvature-selective neurons we report here, however, exhibited at least 2-fold stronger responses to specific CV stimuli than to any other stimulus, including oriented bars or other distinct complex patterns such as corners and crosses. Thus, these curvature-selective neurons can be considered as "curvature detectors" that can detect and signal the presence of a particular CV stimulus. This feature selectivity is akin to that of the "face cells" in the inferotemporal cortex that responded strongly to faces but only weakly to non-face objects [26].

To compare a curvature-selective neuron's preference to curvatures over its preference to OT stimuli, we calculated a curvature preference index (PI_{CV}) = $\max(R_{CV}) / \max(R_{OT})$ for each curvature-selective neuron ([Figures 2H](#) and [2J](#)). Here the $\max(R_{CV})$ was the maximum response to any CV stimuli,

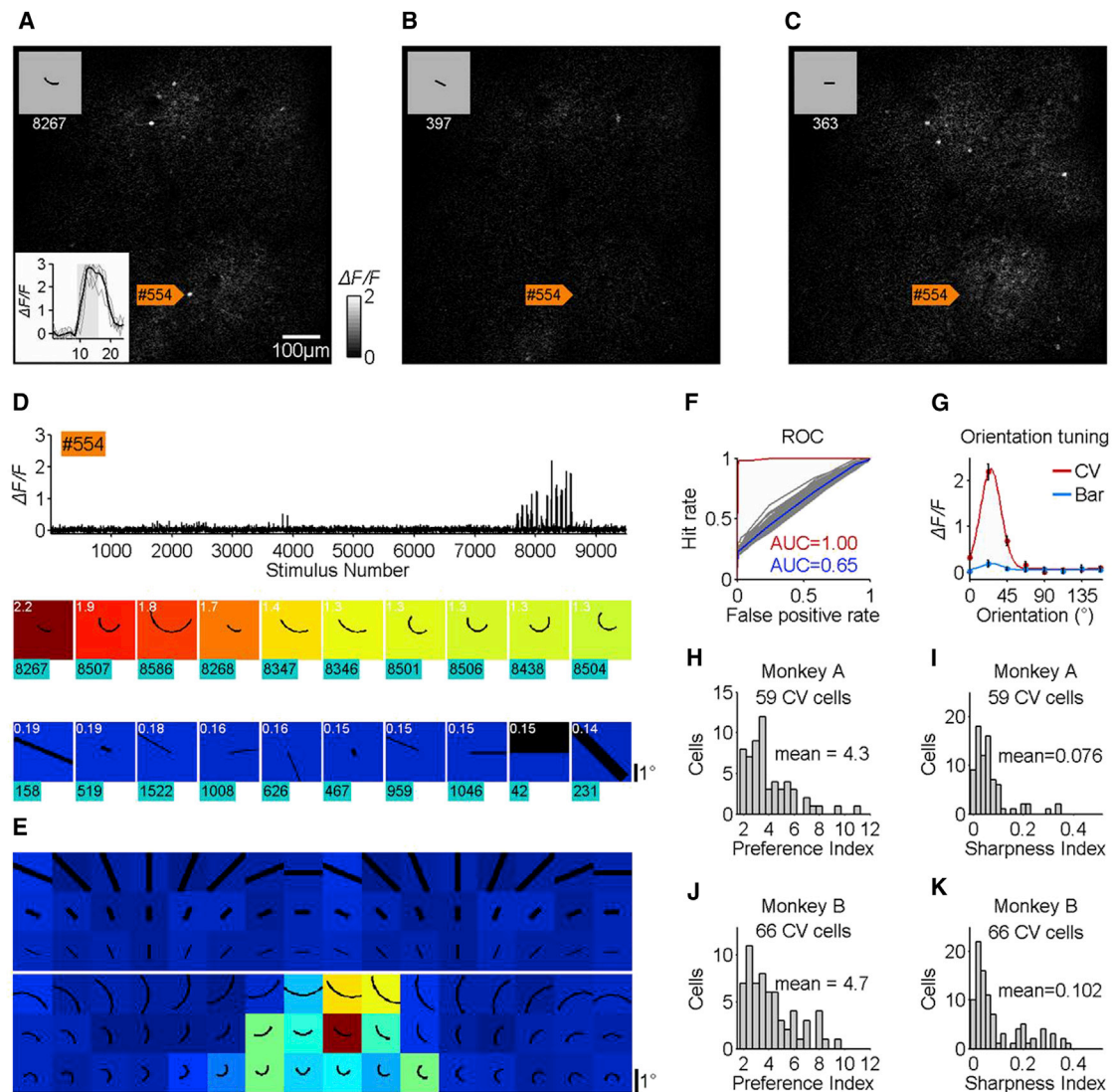


Figure 2. A V1 Superficial Layer Neuron that Is Highly Selective to Curvature

(A–C) Calcium activities, at single-cell resolution, of the imaged V1 superficial layer in responding to a short arc (A, stimulus 8,267) and two short-oriented bars (B and C, stimuli 397 and 363), respectively, from monkey A. The arc strongly activated a few neurons including cell 554.

(D) Responses of cell 554 to the 9,500 artificial stimulus set. The background color of each stimulus indicates the response to the stimulus, proportional to the white $\Delta F/F_0$ number labeled in the upper left corner of each stimulus. All the preferred stimuli of cell 554 (with responses $>50\%$ max) are CV stimuli.

(E) The curvature and orientation tunings of cell 554.

(F) ROC analysis confirmed that the selective responses of cell 554 were reliable and repeatable.

(G) Orientation tuning to the optimal CV stimuli of cell 554 as compared to the orientation tuning to the optimal bar stimuli showed that responses to CV stimuli were much stronger than the responses to the optimally oriented bar stimuli for this neuron. Error bars, mean \pm SEM.

(H) The distribution of curvature preference indices of the curvature-selective cells from monkey A.

(I) The distribution of the sharpness indices of the curvature-selective cells of monkey A. The sharpness index is equivalent to the half-height tuning bandwidth or the percentage of CV stimuli evoking responses above half of the maximum response.

(J and K) The distribution of curvature preference indices (J) and the sharpness index (K) of the curvature-selective cells of monkey B.

See also [Figure S3](#) and [Movie S2](#).

and the $\max(R_{OT})$ was the maximum response to any of the OT stimuli. We found that the curvature-selective neurons responded on average 4.3 and 4.7 times better to the optimal CV stimulus than the optimal OT stimulus, including bars with different lengths. Thus, this observed curvature-selective response could not be simply explained by their end-stopping property or orientation tunings.

We also defined a sharpness index to quantify the neurons' sharpness of tuning to CV stimuli ([Figure 2D](#)) as the percentage of CV stimuli evoking responses above half of the maximum response of the 3×16 curvature parameter table (see [Figure S1](#)) that contained the CV stimulus that evoked the maximum response. The sharpness indices, or the half-height tuning bandwidth of the curvature-selective neurons, had similar

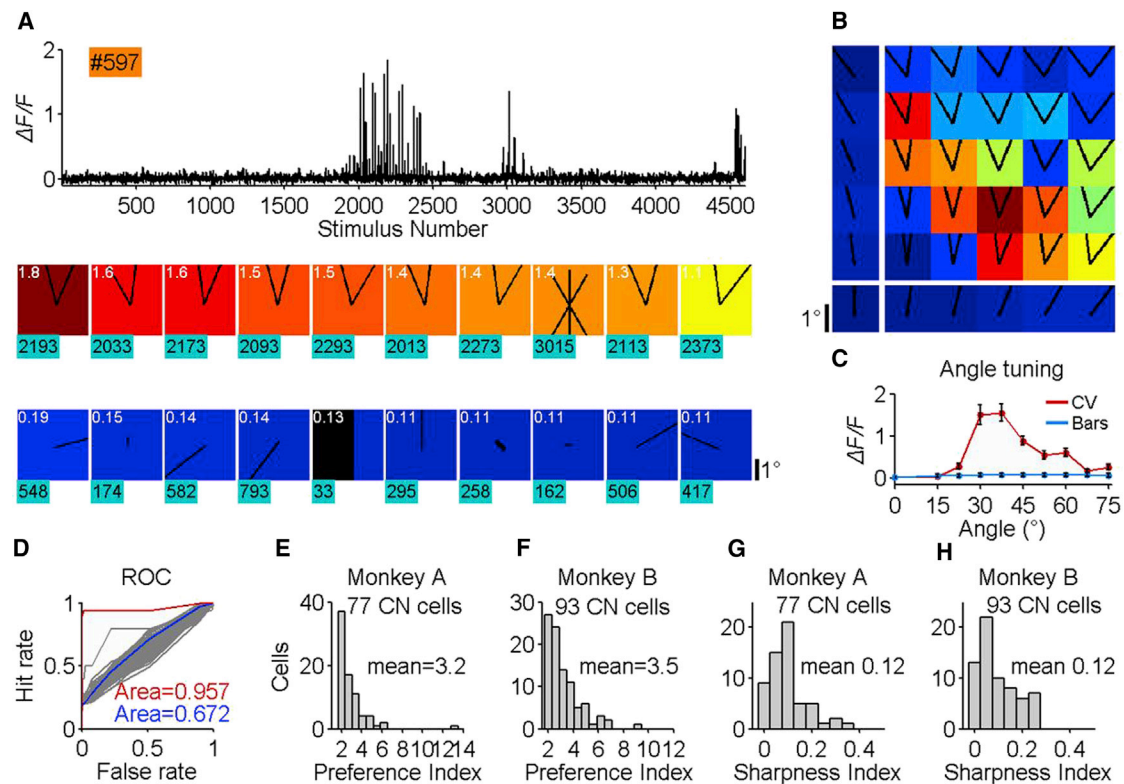


Figure 3. A V1 Superficial Layer Neuron Highly Selective to CN Stimuli

(A) Selective responses of cell 597 from monkey B to the 4,605 stimulus set. The background color of each stimulus indicates the response to the stimulus, proportional to the white $\Delta F/F_0$ number labeled in the upper left corner of each stimulus. All the preferred stimuli (with responses $>50\%$ max) of cell 597 belong to the corner category.

(B) The neuron is selective and tuned to a particular region of the corner parametric space. The response to each preferred whole corner is greater than the sum of the responses to its parts (shown on the left and bottom margins).

(C) Responses to the different orientation of the optimal CN stimuli versus that of the optimal bar stimulus indicates the cell responded more strongly to CN stimuli. Error bars, mean \pm SEM.

(D) ROC analysis confirming the reliability of the selective responses of the cell across trials.

(E and F) The distribution of corner preference indices of corner-selective cells of monkey A (E) and monkey B (F).

(G and H) The distribution of the selectivity sharpness indices of corner-selective cells of monkey A (G) and monkey B (H).

distributions with means of 7% and 12% for monkeys A and B, respectively (Figures 2I and 2K). That is, of the 48 CV stimuli in the curvature parameter table of a particular cue that contained the maximum responding stimulus, approximately three to five stimuli responded above half of the peak response.

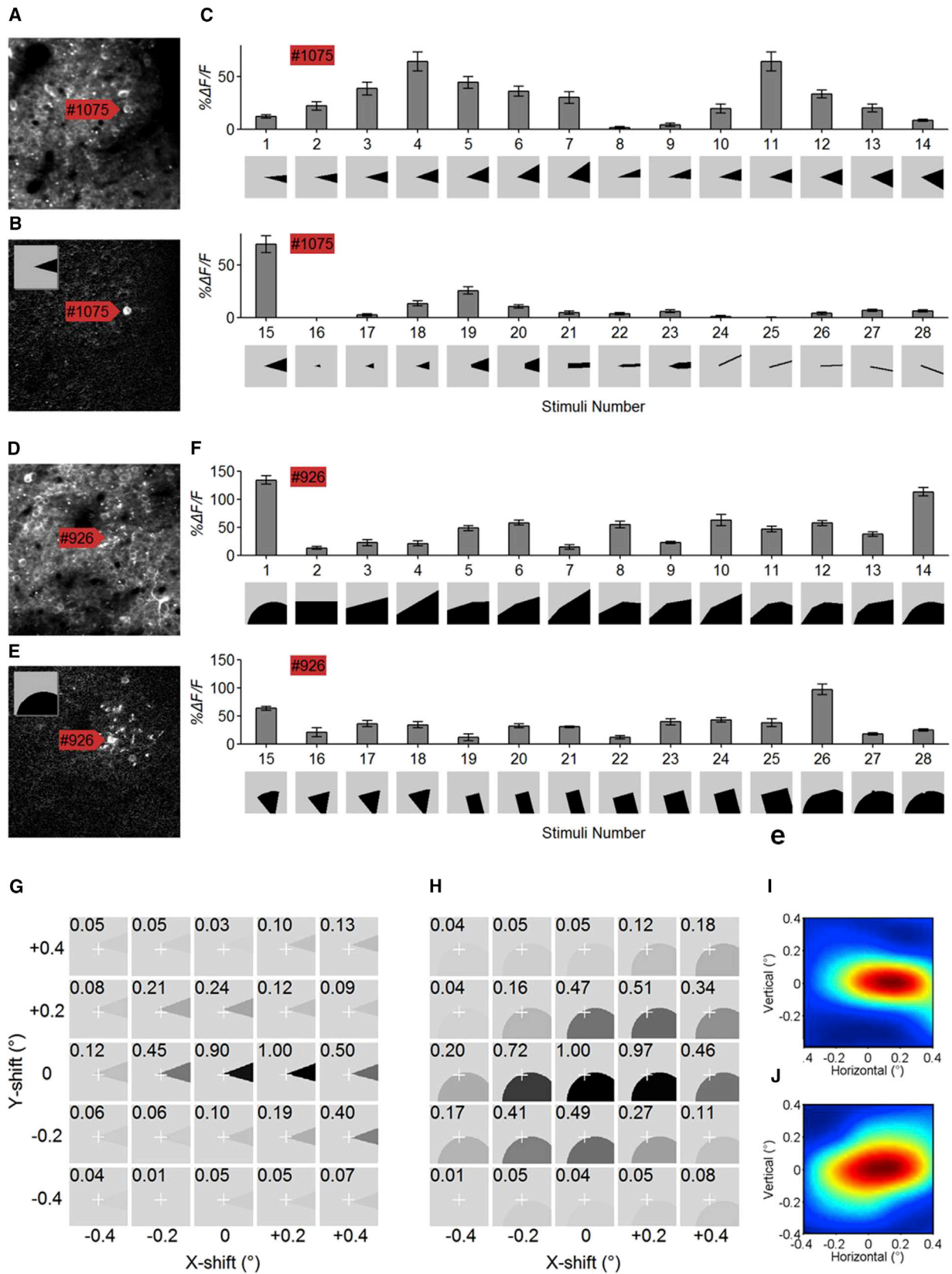
Another example neuron (cell 597) from monkey B responded selectively to CN stimuli (Figure 3). This neuron preferred CN stimuli or stimuli containing corners (e.g., the cross stimulus 3,015 shown in Figure 3A). We defined such cells as “corner-selective cells.” This neuron exhibited systematic tuning to corner parameters (Figure 3B), and its responses were significantly greater to corners than to the component bars alone (Figure 3C). Note that the strict criterion of requiring a corner-selective neuron to respond twice stronger to a preferred CN stimulus than OT stimuli implies that the response of a corner-selective cell to its preferred corner is always greater than the sum responses to the orientation components, which were included in the tested OT set.

In total, we found 77 and 93 such corner-selective cells in monkeys A and B, respectively. More than 94% cells passed

the ROC significance check ($p < 0.001$; Figure 3D). The distributions of the corner preference index $PI_{CN} = (\max(R_{CN}) / \max(R_{OT}))$ for the corner-selective neurons in the two monkeys are shown in Figures 3E and 3F, where $\max(R_{CN})$ was the maximum response to any CN stimuli and $\max(R_{OT})$ was the neuron’s maximum response to any of the OT stimuli. The corner-selective neurons’ responses to the optimal CN stimulus were on average 3.2 (monkey A) and 3.5 (monkey B) times more than their responses to the optimal OT stimuli. We calculated the selectivity sharpness index, or the half-height corner-tuning bandwidth, in corner parameter space. Two monkeys had close sharpness distributions (Figures 3G and 3H).

Validation of HO Stimulus Selectivity with Feature Reduction and Perturbation Experiments

We performed detailed feature reduction and perturbation experiments to identify the critical features of four typical complex pattern-selective neurons in monkey A. We tested a large number of variations of patterns possible in the HO feature space for each tested neuron. For example, in feature reduction,



(legend on next page)

a curvature feature would be simplified to oriented edges or corners. In perturbation, the orientation of each side of a corner could be changed independently. Those experiments could take multi-sessions (days) for each neuron. During these experiments, we verified the stability of targeted neurons by their stable responses to the optimal patterns across sessions.

One example, cell 1,075 from monkey A, was selective to a sharp corner with specific angle and orientation (stimuli 4 and 11, [Figures 4A–4C](#)). Perturbing the orientation of either side of the corner reduced the magnitude of the cell's responses (stimuli 1–15), which indicated that the selectivity of this neuron did not arise from simple orientation tuning to the individual side edges but from the conjunction of both edges. While this neuron did exhibit orientation tuning, its optimal responses to orientation edge or bar stimuli were much weaker compared to those of the optimal corner ([Figure 4C](#), stimuli 15 and 24–28). We also found that deleting part of the CN stimuli, such as the base (stimuli 16–18), the tip (stimuli 19 and 20), or the shoulder (stimuli 22 and 23), all reduced the responses of the neuron significantly. These observations together confirmed that the neuron's selectivity was toward the CN stimulus as a whole, rather than the lower-order features or fragments.

In another example, we identified the critical feature of a curvature-selective cell (926) in monkey A using feature reduction. We found that simplifying the preferred curvature edges to oriented edges ([Figure 4F](#), stimuli 2–4 and 16–25) significantly reduced the neuron's response. HO stimuli like corners or triple-orientation edges restored the responses somewhat ([Figure 4F](#), stimuli 2–4 and 5–13). In addition, replacing the straight edge inside the receptive field with a smooth convex edge almost fully restored the neuronal responses ([Figure 4F](#), stimulus 14). Cutting off the flank of the optimal curved edge stimulus to 0.8° in width resulted in a reduction of the neuron's response by half ([Figure 4F](#), stimulus 15), and additional removal of the flank caused further response decrease (stimuli 16–18). All narrow-oriented edges (0.2° – 0.8° in width, and presented at three positions) could not elicit strong responses (stimuli 19–25), indicating that strong curvature-selective responses might not simply be due to the end-stopping in orientation tunings. Finally, filling two flanks of the narrow-oriented edge with curvature edges largely restored the response (stimulus 26), underscoring the importance of the entire pattern of the stimuli in shaping the pattern

selectivity of the neuron. This was true even in cases where the pattern was larger than the classical receptive field of the neuron. Interestingly, a tiny bump or indent at the critical local position inside the receptive field almost completely annihilated the responses of the neuron ([Figure 4F](#), stimuli 27 and 28), probably due to a break in the smoothness of the curvature. These results confirmed the selectivity of this neuron to a smooth, curved edge with a certain spatial extent.

In the perturbation experiment, we additionally presented the preferred stimuli in a 5×5 grid with 0.2° displacement to map the receptive fields of the cells with their preferred stimuli ([Figures 4G–4J](#)). We found that while the optimal pattern was relatively large ($>0.8^\circ$ in size), the cell was nevertheless sensitive to a 0.2° positional shift of the optimal stimulus.

The Diversity and Complexity of Neuronal Selectivity

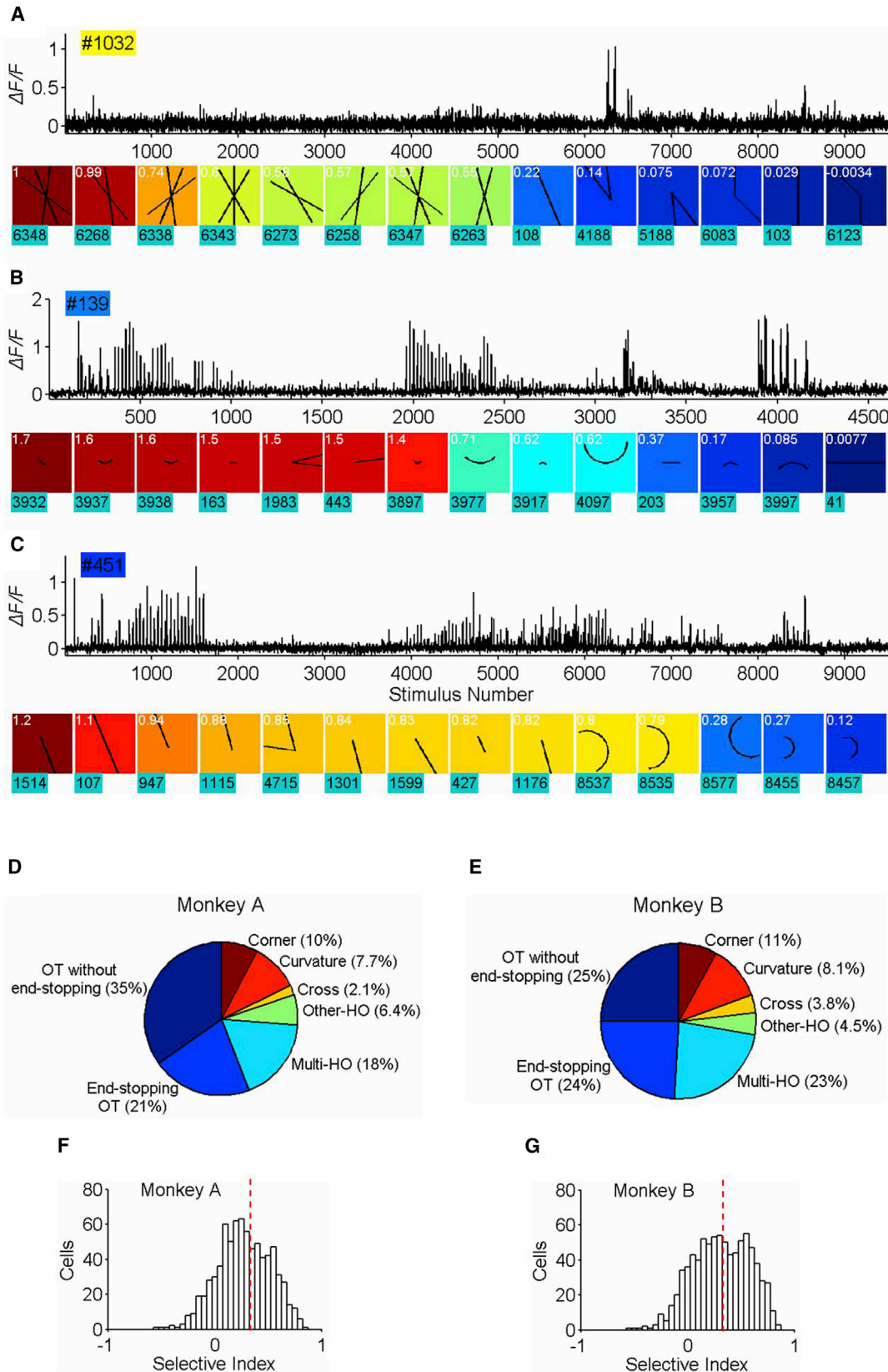
We also found cells that were selective to other categories of complex patterns. Cell 1,032 in monkey A responded selectively to the CX stimuli ([Figure 5A](#)). It responded well to crosses defined by two or three intersecting lines, but not to corners (L junctions) or any individually oriented components. More example cells with HO shape selectivity are shown in [Figure S4](#).

We also found many neurons responding well to oriented bars labeled as orientation-tuned neurons in this study. However, many of these neurons also exhibited tunings to complex features. Nevertheless, to be conservative in our estimate, our strict classification criterion was biased in favor of the lower-order category. Neurons with responses to any OT stimulus over 50% of their individual peak responses would be classified as an OT neuron even though they might also respond strongly to curvature. A case in point, cell 139 in monkey B responded strongly to curvature ([Figure 5B](#), stimuli 3,932, 3,937, and 3,938) and exhibited significant curvature tunings ([Figure 5B](#), stimuli 3,932 versus 3,917 and 3,937 versus 3,957; ANOVA, $p < 0.001$). However, we classified it as an orientation neuron because it responded sufficiently well to short-oriented bars (stimuli 163 and 443). Overall, we found about 80% of the end-stopping orientation-tuned cells had significant curvature tunings (ANOVA, $p < 0.05$). This subgroup of cells could be end-stopping cells with curvature tunings studied in previous studies [[14](#), [15](#)].

However, we found that about 80% of the orientation-tuned cells without end-stopping would also exhibit significant

Figure 4. Feature Reduction and Perturbation Experiments

- (A) A $2 \times$ zoom of baseline F_0 image of a local area (top).
 (B) The differential image $F - F_0$ of the same area in response to visual stimulation of a sharp corner. Cell 1,075 was the most rigorously responding neuron in this image.
 (C) Cell 1,075 was sensitive to the orientations of the two edges of the optimal CN stimulus (perturbations 1–14). Optimal response was elicited by stimulus 15, which was significantly attenuated by removing the sharp tips (stimuli 19 and 20), removing the body part of the pattern (stimuli 16–18, 22, and 23), or modifying other parts of the pattern.
 (D and E) A $2 \times$ zoom of F_0 (D) and $F - F_0$ (E) images in response to the edge of a black circular disk in another imaged region. Cell 926 was the most excited neuron in response to the black disk's curved edge.
 (F) Cell 926 did not respond well to straight edges that are local approximations of the circular edge of the black disk inside the receptive field (stimuli 2–4 and 19–25). Bending the straight line into an angle (stimuli 5, 8, 10–14) to successively better approximate the circular edge increased the neuron's response. Cutting off fragments from the global curvature pattern reduced the responses significantly (stimuli 15–18 and 26). Introducing a small bump or dent at the critical part of the circular edge eliminated its response (stimuli 27 and 28). This feature reduction experiment suggested a smooth global curvature is a critical feature for driving this cell. Error bars, mean \pm SEM.
 (G–J) The spatial receptive fields of the two neurons mapped by their respective optimal stimuli, showing that the neurons were not only highly selective in their preferred features but also highly sensitive to their precise spatial locations. The responses were normalized to between 0 and 1 in (G) and (H), and the contrast of the pattern indicates the strength of the response for visualization purpose.



(legend on next page)

curvature tunings (ANOVA, $p < 0.05$). As an example, cell 451 in monkey A (Figure 5C) responded well to the long-oriented line (stimulus 107), hence it was not end-stopping. Nevertheless, it preferred one curvature (stimulus 8,537) over the opposite curvature containing the same local orientation fragment (stimulus 8,577; ANOVA, $p < 0.01$). Therefore, V1 neurons that were classified as orientation-tuned cells with or without end-stopping could also be tuned to more complex features.

We grouped all the analyzed cells (765 cells from monkey A and 816 cells from monkey B) into two classical orientation-tuned classes (with and without end-stopping) and five HO classes (i.e., curvatures, corners, crosses, compositions, and mixed), using the same criteria that were used in classifying the curvature- or corner-selective cells (Figures 5D and 5E). The mixed class consisted of neurons that responded equally well to stimuli in at least two HO classes, such as both curvature and corner.

Overall, nearly half of the analyzed cells exhibited selectivity to complex patterns over simple oriented features (44% in monkey A and 51% in monkey B). We used an HO-selective index, $SI = (\max(\text{HO}) - \max(\text{OT})) / (\max(\text{HO}) + \max(\text{OT}))$, to characterize the preference to HO patterns against OT stimuli, where $\max(\text{OT})$ is the optimal response to any oriented bar or grating stimuli in the set and $\max(\text{HO})$ is the optimal response to the HO stimuli. Nearly half of the cells showed strong preferences ($SI > 0.33$) for HO stimuli.

In this study, because of the larger number of stimuli we were scanning every day, the number of repeats per stimulus was typically limited to five. The long duration of stimulus of 1 s allowed a long integration window for the cGAMP5 signals. The signal reliability could be comparable to those from 10 to 20 repeats in electrode recording studies.

DISCUSSION

We performed large-scale two-photon imaging of the responses of V1 neurons to an extensive set of stimuli in awake macaques. The results provided a more comprehensive view of the population activities of neurons and a more detailed assessment of the neurons' tuning properties compared to that of single-unit or multi-unit array recordings. In particular, the results revealed that a large portion of neurons in the superficial layer of V1 exhibited strong selectivity to a diverse set of complex patterns. We suggest that these neurons may serve as "local detectors"

for curvatures, corners, junctions, and other HO patterns in the visual object recognition hierarchy.

Previous Studies on V1 Neuronal Coding

V1 neurons are traditionally assumed to primarily encode oriented edges and bars [1], and HO visual features are thought to be represented by neurons in the downstream extra-striate cortical areas, such as V2, V4, and beyond [7–10], building on the elementary-oriented feature detectors in V1.

However, a number of earlier studies suggested that V1 neurons might be more complex than simple linear or nonlinear filters (e.g., linear-nonlinear-poisson [LNP] models) [14–19]. But those works did not provide direct evidence demonstrating V1 neurons' high degrees of selectivity to complex patterns, nor did they necessarily lead to the conclusion that V1 neurons could potentially function as specific pattern detectors. In fact, Hubel and Wiesel found many V1 neurons hard to characterize and called them hypercomplex cells in their pioneer work [13]. End-stopping later became a key attribute of these hypercomplex cells and has been proposed to be used for curvature computation [14, 15]. An early study suggested that V1 cells could detect local orientation discontinuity [16]. Another study suggested V1 neurons may be selective to complex patterns [17], but insufficient stimuli were tested as controls to rule out definitively simple orientation component and end-stopping as potential causes. Only when we tested so many neurons with such a large array of stimuli were we able to discover the complex pattern selectivity of V1 neurons.

Investigation of V1 Neuronal Selectivity

Indeed, our current understanding on V1 neurons' tunings could be biased and limited by both the neurons that could be sampled and the stimuli that could be tested [20, 21]. As shown in this study, the neurons in the superficial layer of V1 were densely packed. It may be very hard to isolate these neurons from extracellular microelectrode recordings.

Meanwhile, the tuning and selectivity of V1 neurons that can be observed also depend on the stimuli tested. For instance, cell 926 from monkey A responded weakly or moderately to oriented edges, exhibiting statistically significant orientation tuning (Figure 4F, stimuli 2–4) and end-stopping (Figure 4F, stimulus 3 versus stimulus 24). We found that even though HO neurons exhibited significantly weaker responses to oriented stimuli than to the optimal HO patterns, most of them did show

Figure 5. Diversity of Feature Selectivity of Neurons in V1 Superficial Layer

(A) Cell 1,032 from monkey A was highly selective to cross patterns. The response of the cell to the optimal CX stimulus was at least twice stronger than stimuli in all other categories, including orientation and corners.

(B) Cell 139 from monkey B responded strongly to a short bar and hence was classified as an end-stopping orientation-tuned cell. Nevertheless, this cell responded strongly to CV stimuli (stimuli 3,932, 3,937, and 3,938), which contained locally oriented features that matched the optimally oriented bars (stimuli 163 and 443), but it was also sensitive to the direction and the degree of the CV stimuli. This example demonstrated that some standard end-stopping orientation-selective neurons could encode curvature, as suggested by earlier studies.

(C) An orientation-tuned cell (451) from monkey A that responded to many different types of stimuli that contain the appropriate orientation element. The cell was not end-stopping. Yet it was tuned to curvature, showing a robust response to CV stimulus 8,537 but a weak response to a flipped curvature (stimulus 8,577, $p < 0.01$), even though both stimuli shared the optimal locally oriented element preferred by the cell.

(D and E) Pie charts of the proportion of each class of feature-selective neurons for monkey A (D) and monkey B (E). Color scheme is as follows: angle/corner, crimson; curvature, red; crosses, yellow; composition, green; mixture, light blue; orientation tuned with end-stopping, blue; and orientation tuned without end-stopping, dark blue.

(F and G) Distributions of the HO feature selectivity of the neuronal population in monkey A (F) and monkey B (G).

See also Figure S4.

significant orientation tuning (>70%; ANOVA, $p < 0.05$). When tested with simple OT stimuli, the HO cells and OT cells had similar distributions of orientation tunings and end-stopping properties. Their orientation tuning and end-stopping properties were also consistent with those from early extracellular recording studies [27]. For cell 926, when tested with multiple orientation segments, it would show contextual modulation effects (Figure 4F, stimulus 6, 10, or 12) or “supra-optimal” responses to orientation discontinuity [16]. Only when we tested richer stimuli containing the appropriate CV stimulus could we discover the cell’s true preference and recognize its high degree of selectivity. Additionally, in some extreme cases, highly selective neurons (such as cell 554 from monkey A, Figure 2D) might be quite silent to non-optimal stimuli, thus easy to miss in previous studies [20, 21]. Given the diversity and the specificity in V1 neuronal selectivity as observed in our study, a rich set of stimuli may always be necessary to efficiently activate individual V1 neurons and find out their true selectivity.

Underlying Mechanisms of V1 Neuronal Selectivity

There is evidence that recurrent interactions might play a role in shaping the stimulus selectivity of V1 neurons [28, 29]. Neurons’ responses become sparser when natural images or movies are shown in full view than through an aperture, suggesting that image context may enhance the “selectivity” of the neurons [18]. Our feature perturbation experiments showed that an extended part of the optimal pattern might be critical in activating V1 neurons (Figure 4). Thus, the influence of the surrounding context might be more feature specific, as also suggested by a previous study [18], than the conventional iso-orientation surrounding modulation, suggested by other earlier studies [5, 30]. It is known that top-down feedback could also shape neuronal selectivity [31], making neuronal tunings more flexible and dynamic depending on the behavioral tasks. But those effects tend to be subtle (around the 5%–10% level), which could not provide a major contribution in the high selectivity (more than 100%) of V1 neurons. Additional experiments are required to elucidate the underlying mechanisms that give rise to the selectivity to complex features we observed.

Functional Implications

When neural signals flow from V1 to V2, the receptive fields expand and become more invariant, resulting in the feature detectors losing spatial and feature precision due to spatial pooling. Our result indicates that there may be a stage of local complex pattern detection in V1 superficial layer in the visual object recognition hierarchy. Having complex feature detectors before spatial pooling has been shown to be beneficial for object recognition (e.g., a “^” detector for the letter “A”) in neural networks [12, 32], which could happen in the early cortical stage of the visual system.

We should emphasize that while a neuron can be selective to a particular feature with strong response, serving as a specific feature detector, it can still be tuned to many other stimulus features and attributes with moderate and weak responses to encode information in a distributed population code.

Conclusions

With large-scale two-photon calcium imaging of V1 neurons, we can observe a large population of neurons in action, ameliorating

potential sampling biases that have plagued single-unit studies in the past. Our study reveals that many individual V1 neurons exhibit strong selectivity to specific complex patterns and might serve as specific feature detectors. This new finding suggests a stage of local complex feature detection in V1 superficial layer for constructing the visual object recognition hierarchy.

STAR★METHODS

Detailed methods are provided in the online version of this paper and include the following:

- KEY RESOURCES TABLE
- CONTACT FOR REAGENT AND RESOURCE SHARING
- EXPERIMENTAL MODEL AND SUBJECT DETAILS
 - Macaque monkey
- METHOD DETAILS
 - Monkey preparation
 - Behavioral task
 - Eye movement control
 - Visual stimuli
 - Two-photon imaging
 - Imaging data analysis
 - Reliability and repeatability analysis of the signals
 - Strategy for randomization and/or stratification
 - Inclusion and Exclusion Criteria of any Data
- QUANTIFICATION AND STATISTICAL ANALYSIS
- DATA AND SOFTWARE AVAILABILITY

SUPPLEMENTAL INFORMATION

Supplemental Information includes five figures and two movies and can be found with this article online at <https://doi.org/10.1016/j.cub.2017.11.039>.

ACKNOWLEDGMENTS

We are grateful to many colleagues for their insightful discussion and generous help on this paper, in particular Mikko Juusola and Dan Yamins for editing earlier versions of the manuscript and Yi Rao, Yulong Li, Fang Fang, Tony Movhson, Robert Desimone, Tao Letian, Yi Zhang, Anna Wang, James DiCarlo, Cong Yu, and Daniel Kersten for helpful comments on various versions of the manuscript. We thank Wenbiao Gan for the early provision of AAV-GCaMP5 and Peking University Laboratory Animal Center for excellent animal care. We acknowledge the Janelia Farm program for providing the GCaMP5-G construct, specifically Loren L. Looger, Jasper Akerboom, Douglas S. Kim, and the Genetically Encoded Calcium Indicator (GECI) project at Janelia Farm Research Campus Howard Hughes Medical Institute. This work was supported by the National Natural Science Foundation of China (31730109); National Natural Science Foundation of China Outstanding Young Researcher Award (30525016); a project 985 grant of Peking University, National Basic Research Program of China (2017YFA0105201); Beijing Municipal Commission of Science and Technology (Z151100000915070); and NIH 1R01EY022247, NSF CISE 1320651, and IARPA D16PC00007 of the USA.

AUTHOR CONTRIBUTIONS

S.T. conceived the project and designed the experiments. S.T. performed experiments with assistance from M.L., F.L., and H.J. on preparations. Y.Z., B.T., and Y.X. analyzed the data. S.T. and T.S.L. analyzed the data and wrote the paper.

Received: September 20, 2017

Revised: October 30, 2017

Accepted: November 17, 2017

Published: December 14, 2017

REFERENCES

- Hubel, D.H., and Wiesel, T.N. (1959). Receptive fields of single neurones in the cat's striate cortex. *J. Physiol.* **148**, 574–591.
- Jones, J.P., and Palmer, L.A. (1987). An evaluation of the two-dimensional Gabor filter model of simple receptive fields in cat striate cortex. *J. Neurophysiol.* **58**, 1233–1258.
- Livingstone, M.S., and Hubel, D.H. (1984). Anatomy and physiology of a color system in the primate visual cortex. *J. Neurosci.* **4**, 309–356.
- Movshon, J.A., Thompson, I.D., and Tolhurst, D.J. (1978). Receptive field organization of complex cells in the cat's striate cortex. *J. Physiol.* **283**, 79–99.
- Knierim, J.J., and van Essen, D.C. (1992). Neuronal responses to static texture patterns in area V1 of the alert macaque monkey. *J. Neurophysiol.* **67**, 961–980.
- Das, A., and Gilbert, C.D. (1999). Topography of contextual modulations mediated by short-range interactions in primary visual cortex. *Nature* **399**, 655–661.
- Anzai, A., Peng, X., and Van Essen, D.C. (2007). Neurons in monkey visual area V2 encode combinations of orientations. *Nat. Neurosci.* **10**, 1313–1321.
- Connor, C.E., Brincat, S.L., and Pasupathy, A. (2007). Transformation of shape information in the ventral pathway. *Curr. Opin. Neurobiol.* **17**, 140–147.
- Gallant, J.L., Braun, J., and Van Essen, D.C. (1993). Selectivity for polar, hyperbolic, and Cartesian gratings in macaque visual cortex. *Science* **259**, 100–103.
- Kobatake, E., and Tanaka, K. (1994). Neuronal selectivities to complex object features in the ventral visual pathway of the macaque cerebral cortex. *J. Neurophysiol.* **71**, 856–867.
- LeCun, Y., Bengio, Y., and Hinton, G. (2015). Deep learning. *Nature* **521**, 436–444.
- Riesenhuber, M., and Poggio, T. (1999). Hierarchical models of object recognition in cortex. *Nat. Neurosci.* **2**, 1019–1025.
- Hubel, D.H., and Wiesel, T.N. (1968). Receptive fields and functional architecture of monkey striate cortex. *J. Physiol.* **195**, 215–243.
- Dobbins, A., Zucker, S.W., and Cynader, M.S. (1987). Endstopped neurons in the visual cortex as a substrate for calculating curvature. *Nature* **329**, 438–441.
- Ponce, C.R., Hartmann, T.S., and Livingstone, M.S. (2017). End-stopping predicts curvature tuning along the ventral stream. *J. Neurosci.* **37**, 648–659.
- Sillito, A.M., Grieve, K.L., Jones, H.E., Cudeiro, J., and Davis, J. (1995). Visual cortical mechanisms detecting focal orientation discontinuities. *Nature* **378**, 492–496.
- Hegd e, J., and Van Essen, D.C. (2007). A comparative study of shape representation in macaque visual areas v2 and v4. *Cereb. Cortex* **17**, 1100–1116.
- Vinje, W.E., and Gallant, J.L. (2000). Sparse coding and decorrelation in primary visual cortex during natural vision. *Science* **287**, 1273–1276.
- Victor, J.D., Mechler, F., Repucci, M.A., Purpura, K.P., and Sharpee, T. (2006). Responses of V1 neurons to two-dimensional hermite functions. *J. Neurophysiol.* **95**, 379–400.
- Olshausen, B.A., and Field, D.J. (2005). How close are we to understanding v1? *Neural Comput.* **17**, 1665–1699.
- Carandini, M., Demb, J.B., Mante, V., Tolhurst, D.J., Dan, Y., Olshausen, B.A., Gallant, J.L., and Rust, N.C. (2005). Do we know what the early visual system does? *J. Neurosci.* **25**, 10577–10597.
- Denk, W., Strickler, J.H., and Webb, W.W. (1990). Two-photon laser scanning fluorescence microscopy. *Science* **248**, 73–76.
- Li, M., Liu, F., Jiang, H., Lee, T.S., and Tang, S. (2017). Long-term two-photon imaging in awake macaque monkey. *Neuron* **93**, 1049–1057.e3.
- Akerboom, J., Chen, T.W., Wardill, T.J., Tian, L., Marvin, J.S., Mutlu, S., Calder n, N.C., Esposti, F., Borghuis, B.G., Sun, X.R., et al. (2012). Optimization of a GCaMP calcium indicator for neural activity imaging. *J. Neurosci.* **32**, 13819–13840.
- Quiroga, R.Q., Reddy, L., Kreiman, G., Koch, C., and Fried, I. (2005). Invariant visual representation by single neurons in the human brain. *Nature* **435**, 1102–1107.
- Bruce, C., Desimone, R., and Gross, C.G. (1981). Visual properties of neurons in a polysensory area in superior temporal sulcus of the macaque. *J. Neurophysiol.* **46**, 369–384.
- Ringach, D.L., Shapley, R.M., and Hawken, M.J. (2002). Orientation selectivity in macaque V1: diversity and laminar dependence. *J. Neurosci.* **22**, 5639–5651.
- Haider, B., Krause, M.R., Duque, A., Yu, Y., Touryan, J., Mazer, J.A., and McCormick, D.A. (2010). Synaptic and network mechanisms of sparse and reliable visual cortical activity during nonclassical receptive field stimulation. *Neuron* **65**, 107–121.
- Nassi, J.J., Lomber, S.G., and Born, R.T. (2013). Corticocortical feedback contributes to surround suppression in V1 of the alert primate. *J. Neurosci.* **33**, 8504–8517.
- Sceniak, M.P., Hawken, M.J., and Shapley, R. (2001). Visual spatial characterization of macaque V1 neurons. *J. Neurophysiol.* **85**, 1873–1887.
- McManus, J.N.J., Li, W., and Gilbert, C.D. (2011). Adaptive shape processing in primary visual cortex. *Proc. Natl. Acad. Sci. USA* **108**, 9739–9746.
- Fukushima, K. (1980). Neocognitron: a self organizing neural network model for a mechanism of pattern recognition unaffected by shift in position. *Biol. Cybern.* **36**, 193–202.

STAR★METHODS

KEY RESOURCES TABLE

| REAGENT or RESOURCE | SOURCE | IDENTIFIER |
|--|-----------------------|---|
| Experimental Models: Organisms/Strains | | |
| Rhesus monkeys | Beijing Prima Biotech | http://www.primasbio.com/cn/Default |
| Recombinant DNA | | |
| AAV1.hSyn.GCaMP5G | Penn Vector Core | V5072MI-R |
| Software and Algorithms | | |
| MATLAB | MathWorks | MATLAB 7.12.0 (R2011a) |
| Codes for the movement correction | This paper | https://github.com/Tangshm/V1-Pattern-Selectivity/projects/1 |

CONTACT FOR REAGENT AND RESOURCE SHARING

Further information and requests for reagents may be directed to and will be fulfilled by the Lead Contact, Shiming Tang (tangshm@pku.edu.cn).

EXPERIMENTAL MODEL AND SUBJECT DETAILS

Macaque monkey

The rhesus monkeys were purchased from Beijing Prima Biotech Inc and housed at Peking University Laboratory Animal Center. The study used two health adult male monkeys, 4–5 years of age and weighing 5–7 kg. All experimental protocols were approved by the Peking University Animal Care and Use Committee.

METHOD DETAILS

Monkey preparation

Two sequential surgeries were performed on each animal under general anesthesia and strictly sterile conditions. In the first surgery, a 16-mm hole was drilled in the skull over V1. The dura was opened, and 50 to 100 nL of AAV1.hSynap.GCaMP5G.WPRE.SV40 (AV-1-PV2478, titer 2.37e13 (GC/mL), Penn Vector Core) were pressure-injected at a depth of ~500 μ m. After AAV injection, the dura was sutured. The removed skull bone was placed back and the scalp was sutured. The animal was then returned to its cage for recovery and was administered an antibiotic (Ceftriaxone sodium, Youcare Pharmaceutical Group, China) for one week. After 45 days, a second surgery was performed, in which three head-posts were implanted on the animal's skull, two on the forehead and one on the back of the head. A T-shaped steel frame was connected to these head posts for head stabilization during imaging. The skull and dura were opened again. A glass coverslip (diameter 8 mm and thickness 0.17 mm) was glued to a titanium ring and then gently pushed down onto the cortical surface. A ring-shaped GORE membrane (20 mm in outer diameter) was inserted under the dura. The titanium ring was glued to the dura and skull with dental acrylic to form an imaging chamber. The whole chamber, formed by the thick dental acrylic, was then covered by a steel shell to prevent breakage of the coverslip when the animal was returned to the home cage [23].

Behavioral task

During imaging, each monkey was seated in a primate chair with a head restraint and performed a fixation task, which involved fixating on a small white spot (0.1°) within a window of 1° for over 2 s to obtain a juice reward. Eye position was monitored with an infrared eye-tracking system (ISCAN) at 120 Hz.

Eye movement control

We analyzed the distribution of eye-positions during stimulus ON periods. While a 1° fixation window was used, the monkeys' fixations during stimulus presentation (from 1 to 2 s in the graph) were quite stable and precise, with 98% of the eye movement traces within a 0.4° diameter window and 95% of the eye movement traces within a 0.2° window. The standard deviation of the distribution of eye positions during stimulus presentation was less than 0.05°, which was significantly smaller than the typical receptive field sizes of neurons at 3–5° degree eccentricities (ranging from 0.3° to 0.8°). To examine whether the eye movement contributed significantly to the distribution of neuronal population responses, we compared the standard deviations (SDs) of eye positions in different levels of

neuronal population responses to rule out the hypotheses the eye movements could cause differential responses. We considered three classes of population responses: (1) weak responses ($\Delta F/F0 < 0.5$); (2) sparse, strong responses, with a few cells (less than 10) responding strongly ($\Delta F/F0 > 0.5$); and (3) dense responses (more than ten cells responded strongly). We found no statistically significant differences in the distribution of eye position data in these three classes (Figure S5), which indicated that the observed effects are not caused by eye movement differences. In addition, we found the neuronal responses to stimuli were reliable and reproducible across trials (Figure S3). We concluded that the effects of random eye-movement jitters were minimal.

Visual stimuli

Visual stimuli were generated using the ViSaGe system (Cambridge Research Systems) and displayed on a 17" LCD monitor (Acer V173, 80Hz refresh rate) positioned 45 cm from the animal's eyes. Each stimulus was presented for one second following a one-second blank at the beginning of the trial while the monkey fixated. We estimated the RF sizes and positions of the imaged neurons with small drifting gratings (100% contrast square waves, with 4 and 8 cyc/deg at 1 and 2 Hz temporal frequency, 0.8° in diameter), and bars (0.1° by 0.4°) and dots (0.2° by 0.2°) presented at different locations (7 by 7 grids). The RFs were estimated to be between 0.3° to 0.8° in size, located at around 3°-5° in eccentricity for the two monkeys.

A stimulus set containing 7,900 higher-order pattern stimuli and 1,600 simple orientation stimuli of various sizes from 0.4° to 3° was derived from 138 basic patterns (Figure 1), and rotated in 22.5° increments. For both monkeys, a set of orientation bar stimuli were also presented at 7.5° orientation step to sample 48 orientations with the end of the 1.5° bar (the oriented bar components of the corners, see Figure S1B). The 138 basic patterns were divided into 6 classes (simple orientation – gratings and lines; short lines with ends in the receptive fields; angles/corners; crosses; curvatures – circles, rings, and curves; and other complex patterns, see also Figure S1).

Each stimulus was shown at five different locations, one at the center of the receptive field cluster, and four at 0.2° spatial shifts in the four cardinal directions relative to the RF cluster center. This entire stimulus set was divided into 8 subsets, each corresponding to a major rotation of the basic patterns, which required 8 sessions (days) to complete the testing (Figure 1E). For monkey B, we managed to finish half of the OT and HO stimuli (basic patterns at 45° rotation increments). About 6,000 trials were performed in each recording session with at least 5 repetitions obtained for each stimulus. The order of the visual stimuli was randomized across trials in each recording session.

Two-photon imaging

After a recovery period of ten days from the second surgery, the animals were trained to maintain eye-fixation. Two-photon imaging was performed using a Prairie Ultima IV (*In Vivo*) two-photon microscope (Bruker Nano, FMBU, formerly Prairie Technologies) and a Ti: Sapphire laser (Mai Tai eHP, Spectra Physics). The wavelength of the laser was set at 1000 nm. An area of 850 $\mu\text{m} \times 850 \mu\text{m}$ was imaged with a 16 \times objective (0.8-N.A., Nikon). A standard slow galvanometer scan was used to obtain high resolution static images of cells (1024 \times 1024). A fast, resonant scan (up to 32 frames per second) was used to image of neuronal activity. The images were recorded at 8 frames per second by averaging 4 frames each. Even though infected cells at depths of up to 700 μm could be imaged, we found that a layer at a depth of 160 μm to 180 μm contained a high density of infected cells, so we focused on imaging V1 neurons within this depth (180 μm in monkey A and 160 μm in monkey B).

Imaging data analysis

All data analyses were performed using MATLAB (The MathWorks, Natick, MA). The images from each session were first aligned to a template image (the average image of 1000 frames) using a normalized, cross-correlation-based translation algorithm. This alignment corrected the X-Y offset of images caused by the motion between the objective and the cortex. During long-term recordings, image registrations and alignments were performed to match individual cells across different sessions/days using standard image registration software available in MATLAB. These registered images were integrated into one large session for further analysis of shape and feature tuning²². In this experiment, we further confirmed the stability of neuronal population responses across sessions (days) by examining the consistency of population responses to 15 common stimuli in all sessions (Figure S2).

The cell density was high in the superficial layer of V1, and many cell bodies were quite dim at rest. It was difficult to visually identify these cells based on the morphology of static images with the naked eye or by computational algorithms alone. Hence, we identified regions of interest (ROIs) corresponding to the cell bodies based on the neurons' responses. The differential images (averaged frame of the images during the stimulus ON period subtracting that during stimulus OFF period for each stimulus condition) were first filtered using low-pass and high-pass Gaussian filters (5 pixels and 50 pixels, 2 orders, respectively) to emphasize those activity regions matching the cell sizes. Note that these two filters were only used for ROI identifications. In all further analyses, we used raw, unfiltered data. Connected subsets of pixels (> 25 pixels) with average pixel value greater than 3 standard deviations (std) of each differential image were identified as active neurons. Note that this empirical threshold was only used to decide the ROIs of activated cells and was not a cutoff threshold of measuring neuronal responses. A higher threshold would allow the detection and selection of the ROIs of cell bodies more accurately but would miss some weakly responding cells. On the other hand, a lower threshold may include more cells but would have a greater chance of including some false ROIs that cannot be matched to any cell bodies.

The response of a neuron is computed as the ratio of fluorescence change ($\Delta F/F0$) of these ROIs, whereas $\Delta F = F - F0$. $F0$ is the baseline activity during the blank screen prior stimulus onset in each trial, and F is fluorescence activity in the ROI during stimulus presentation in the trial.

Reliability and repeatability analysis of the signals

A key finding of this study is that individual neurons respond strongly to a very select set of stimuli. To ensure the observed specificity and selectivity in neuronal responses are reliable and repeatable across trials rather than from random spurious activities or noises, we performed Receiver Operating Characteristics (ROC) analysis [25] across trials. For each single neuron, we examined whether the highly selective responses ($\Delta F/F_0 > 0.5$ max response) observed were reliable across trials by performing the following ROC analysis. We first set all stimuli that produced strong mean responses greater than the half-maximum mean peak in ON class and all other stimuli in OFF class. We then computed the ROC for classifying the ON class against the OFF class based on the neuronal response in each single trial. If the responses above the half-maximum were stable across all trials, then the AUC (area under the ROC curve) would be close to 1.0 as the ON and OFF classes were readily discriminable. The null hypothesis is that the sparse strong responses arose from the spurious single trial epileptic response in a particular trial, and thus were not repeatable across trials. In this case, the AUC would be close to 0.667. To test this hypothesis, we shuffled all the responses relative to the stimulus labels (see also [Figure S3](#) for details) in each trial, and recomputed the mean responses for all the stimuli across the shuffled trials. We found that most of the shuffled cases had much lower average peak responses as a result of the mismatch of the rigorous sparse responses across trials ([Figure S3](#)), which suggested the strong sparse (highly selective) responses could not have arisen from spurious noise responses, confirming the reliability of the selective responses to a particular stimulus in the original data. We repeated the shuffles and ROC analysis to obtain the AUC for 1,000 times. Notably, in this setting, the random responses would produce an AUC of 0.667 by chance. The probability of the null hypothesis is the percentage of time that the AUCs of the 1,000 shuffles reach the AUC of the original data. We found the probability of the null hypothesis to be less than 0.001 ($p < 0.001$) for cell #554. This confirmed that the curvature selectivity of this cell is stable, and could not result from spurious epileptic responses or false signals. Overall, more than 92% imaged neurons in both monkeys passed this ROC significant check with $p < 0.001$. These results confirmed that the observed specificity in neuronal responses are reliable and repeatable across trials rather than from random spurious firing or noises.

Strategy for randomization and/or stratification

The order of the visual stimuli was randomized during experiments.

Inclusion and Exclusion Criteria of any Data

The weak responded neurons with $\Delta F/F_0 < 0.5$ were excluded during analysis.

QUANTIFICATION AND STATISTICAL ANALYSIS

Statistics were performed using customized MATLAB software. The proportion of orientation tuned cells with curvature tunings were judged by using one-way ANOVA ($p < 0.01$). A spearman correlation coefficient was used to quantify the stability of recordings across days ([Figure S2](#)). Data are presented as mean \pm SEM or as individual data points, as stated in the figure legends. Number of replicates can be found within the figure legends for each experiment.

DATA AND SOFTWARE AVAILABILITY

The neuronal responses data and stimuli used in this study can be found at <https://github.com/TangshM/V1-Pattern-Selectivity/projects/1>.